State Variable Form of Unsteady Airfoil Aerodynamics with Vortex Shedding

Yi Tsung Lee*, Arun Vishnu Suresh Babu †, Matthew Bryant‡, and Ashok Gopalarathnam§
North Carolina State University, Raleigh, NC, USA

This paper presents a state-variable formulation to model and simulate the 2D unsteady aerodynamics of an airfoil undergoing arbitrary motion kinematics. The model builds upon a large-angle unsteady aerodynamic formulation in which the airfoil is represented using a lumped vortex element (LVE) model. The airfoil is divided into several panels, with a bound vortex placed on each panel. At any time instant, the bound-vortex strengths are determined by employing zero-normal-flow conditions at the control points located on each panel. The vorticity shed from the trailing edge of the airfoil is modeled using discrete vortices that move freely in the flow field. The required state variables are first identified, and all the time derivative terms of the state variables are then derived to form the final state-variable representation. Trailing-edge vortex shedding is incorporated using the Kelvin condition. The final state variable equation can be solved as an ordinary differential equation using any standard ODE-solving algorithm. Three case studies are presented here to evaluate the predictions of the model. In the cases considered here, the airfoil undergoes various unsteady plunge motions. The aerodynamic load history and the wake patterns are compared against the results from the low-order model developed by Narsipur et al. [1] in previous research. The comparison shows that the current state-variable formulation captures the unsteady flow characteristics and the aerodynamic load in good agreement with the reference results.

Nomenclature

α	pitch displacement of the airfoil
h	plunge displacement
Γ	vortex strength
Γ_b	bound vortex strength
Γ_{LEV}	LEV vortex strength
Γ_{TEV}	TEV vortex strength
Wn	downwash normal to the airfoil
U_∞	freestream speed
ϕ_W	velocity potential due to free vortices in the wake
ϕ_B	velocity potential due to bound vortices
c	chord
t	dimensional time
t^*	non-dimensional time
LESP	leading edge suction parameter
LDVM	LESP-modulated discrete vortex method
FV	free Vortex
LEV	leading Edge Vortex
TEV	trailing Edge Vortex
DV	discrete Vortex

*Ph.D. student, Department of Mechanical and Aerospace Engineering, ylee26@ncsu.edu
†Postdoctoral Research Scholar, Department of Mechanical and Aerospace Engineering, asuresh2@ncsu.edu
‡Associate Professor, Department of Mechanical and Aerospace Engineering, mbryant@ncsu.edu
§Professor, Department of Mechanical and Aerospace Engineering, Associate Fellow, AIAA

I. Introduction

Unsteady aerodynamics is a field of great research interest due to its wide range of applications in nature and engineering. Many interesting flow phenomena occur on wings undergoing unsteady motion, such as the flow reversal around the trailing edge [2], which exists only when the airfoil starts an abrupt unsteady motion and diminishes when the airfoil and flow field approaches a steady state. The recent interest in bio-inspired flight has driven many studies on live insects and mechanical models of insect wings [3–6]. The results from the earlier studies on such flapping wings revealed the presence of the leading-edge vortex (LEV), which only exists in airfoils undergoing unsteady motion and had never been observed on conventional fixed wings. The existence of LEV quickly drew a lot of interest among engineers and researchers aiming to build small-scale high-lift micro-aerial vehicles (MAVs). The formation and dynamics of LEV has interested not only researchers working on bio-inspired flight, but also the dynamic-stall community. Dynamic stall occurs when an airfoil experiences rapid variations in the angle of attack and is known to result in sudden load fluctuations in applications such as rotary aircraft and wind turbines [7–10]. Dynamic stall usually results in a delay of stall onset and an increase in the maximum lift. This may appear beneficial, but the large fluctuation in the unsteady aerodynamic loads decreases the performance and poses structural and control issues. It is important not only to understand dynamic stall and the associated LEV shedding phenomena, but also to develop models that can accurately predict their effects on wings and airfoils.

A vast amount of work has been done in the field of unsteady aerodynamics using experimental and numerical methods. McCroskey [11, 12] investigated the evolution of the dynamic stall phenomenon and the resulting unsteady aerodynamic forces and moments of airfoils. In experimental works, flow visualization helps to identify the evolution of coherent structures in the flow field during the dynamic stall. The development of advanced pressure sensing techniques has enabled the precise measurement of the pressure distribution on the airfoil surface during dynamic stall [13–15]. These surface pressure studies have revealed the existence of a suction peak near the leading edge of airfoils during dynamic stall. Similar observations have also been made by numerical studies [16, 17] on dynamic stall. In recent research on theoretical modeling of LEVs on airfoils, Ramesh et. al. [18] introduced the concept of the critical leading-edge suction parameter (LESP). It was observed that the initiation of LEV shedding correlates with the LESP reaching a critical value. The critical LESP value for an airfoil at a given Reynolds number is largely independent of the motion kinematics. The critical LESP value for a given airfoil at a given Reynolds number, once determined from CFD or experimental results, can be used in low-order models to predict LEV shedding phenomena and the unsteady loads for that airfoil-Re combination for a variety of motion kinematics.

While experimental and numerical approaches provide us with high-fidelity results, low-order theoretical models are important to further our understanding of the unsteady aerodynamic phenomena. Moreover, they are necessary for fast-prediction of loads for control design and performing preliminary design iterations. The physics-based low-order models capable of simulating LEV shedding, which is regarded as one of the most important flow characteristics, has been addressed by various researchers. Recently, the concept of LESP, combined with a discrete vortex model, has shown promise in simulating the LEV shedding phenomena from airfoils undergoing unsteady motion in uniform [18–20] and nonuniform [21, 22] freestream conditions, tandem airfoil configurations [23, 24], vertical-axis wind turbines [25] and for airfoils with trailing-edge separation [26].

The accuracy of these discrete-vortex-method-based low order models can be improved by using higher-order numerical integration schemes. Moreover, improving the time-stepping methodology can improve the numerical stability of discrete-vortex methods. For example, numerical instabilities have been observed in aeroelastic studies using discrete vortex methods [27] solved with Euler time-stepping scheme. In addition, Ramesh et al. used a loose coupling between the aerodynamic model and the structural model. A tight coupling can be achieved by formulating a unified dynamic model encompassing both the aerodynamic and structural quantities. In this work, we explore the possibility of obtaining a state-variable representation of an existing aerodynamic model, specifically the lumped vortex element (LVE) method developed in the research of Narsipur et al. [1]. We present an approach for reformulating the low-order aerodynamic model into a state variable form. We also discuss the methodology to incorporate unsteady vortex shedding from the trailing edge of the airfoil. The state-variable formulation will have the potential to be used for any higher-order integration algorithms and common ODE solver packages.

Th4 paper is organized as follows: In section. II, the details of the reference unsteady LVE model of Narsipur et al. [1] are discussed. The reformulation of this model into a state-variable form is also presented. In the following section. III, the results from the state-variable model are presented and are compared with the the reference-LVE results for three different plunge motions. Comaprison of the aerodynamic loads, LESP, and the wake patterns are discussed in this section. Finally, the conclusions from the current work are presented in section. IV, along with a discussion of the direction of future research.

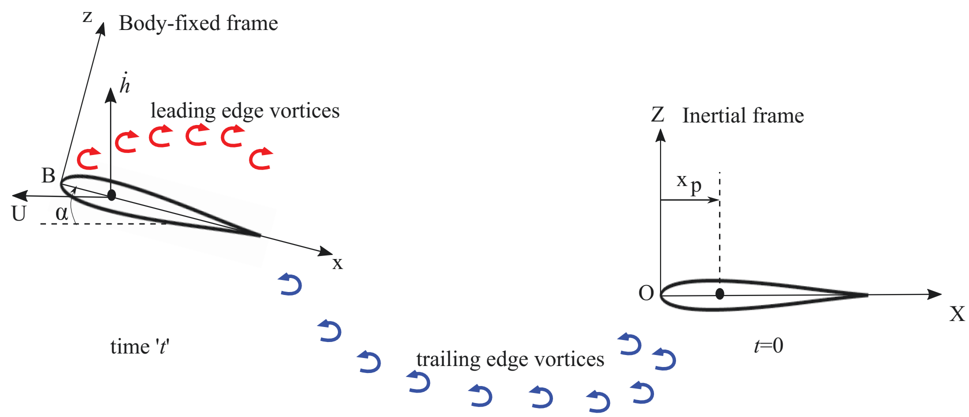

Fig. 1 Illustration of the airfoil kinematics and the discrete vortices shed from it, along with the variables used in the unsteady aerodynamic model

II. Theory

The schematic representation in figure 1 shows an airfoil of chord c undergoing arbitrary prescribed pitching and heaving kinematics. The kinematic state of the airfoil is defined by the pitch angle α, the heave position h, and the respective velocities $\dot{\alpha}$ and $\dot{h}$. The pivot point, located at a distance x_p aft of the leading edge, denotes the center of rotation of the airfoil. Also shown is a body-fixed frame Bxz, with the origin coinciding with the leading edge of the airfoil and the x and z axes extending in the chord-wise and chord-normal directions, respectively. The wake of the airfoil consists of discrete LEVs and trailing-edge vortices (TEVs) shed from either edge of the airfoil in the previous time steps.

A. Lumped Vortex Element model and the Unsteady Thin Airfoil Theory

The Lumped Vortex Element (LVE) method assumes that the airfoil can be represented by several bound vortex elements concentrated on points along the camberline of the airfoil. The airfoil can be cut into several panels, with each bound vortex concentrating on the quarter-chord position of the panel as a discrete bound vortex element, and for each panel, a control point is also defined at the three-quarter-chord position of the panel. The total bound vortex sheet strength is represented by Γ. The zero-normal-flow condition can be written as

$$\left(\nabla\phi_B + \nabla\phi_w + \vec{U_0} - \vec{U}_{rel} - \dot{\alpha} \times \vec{r}\right) \cdot \vec{n} = 0 \tag{1}$$

In this equation, the $\nabla\phi_B$ is the velocity induced due to the velocity potential from bound vortex elements, while $\nabla\phi_w$ is the velocity induced due to all the wake, or called free vortices. The $\vec{U_0}$ is the free stream velocity vector, $\vec{U}_{rel}$ is the translational velocity of the airfoil, and $\dot{\alpha} \times \vec{r}$ is the velocity induced due to the airfoil pitch motion, with $\dot{\alpha}$ meaning the pitch angular velocity and $\vec{r}$ is the position vector of a point on the airfoil relative to the pivot point. In the LVE method, this equation is valid on the control point of every panel. It states that at every control point, the sum of the velocity normal to the panel from the bound vortices, free vortices, free stream, and motion kinematics should balance each other and result in zero normal flow at every control point. Equation (1) will then be written as:

$$\nabla\phi_B \cdot \vec{n} = -\left(\nabla\phi_w + \vec{U_0} - \vec{U}_{rel} - \dot{\alpha} \times \vec{r}\right) \cdot \vec{n} = -Wn \tag{2}$$

In this equation, the left-hand side can be regarded as the self-induced velocity normal to the panel, which is the sum of induced velocity resulting from all the bound vortex elements at each control point. The right-hand side, Wn, represents the downwash normal to the panel at each control point. The induced velocity along the x and z directions can be expressed using the Biot-Savart law as:

$$u_i = \frac{\Gamma_j}{2\pi r_{ij}^2}(z_i - z_j) \tag{3}$$

$$w_i = -\frac{\Gamma_j}{2\pi r_{ij}^2}(x_i - x_j) \tag{4}$$

$$r_{ij}^2 = \sqrt{\left((x_i - x_j)^2 + (z_I - z_j)^2\right)^2 + \delta v_{core}^4} \tag{5}$$

This equation gives the induced velocity $\vec{u}_i$ at position $\vec{x}_i$ due to the vortex at $\vec{x}_j$ with vortex strength Γ_j. The distance between the point i and point j is defined using Equation (5), with a special term δv_{core}^4. The value of δ will be zero when the distance is calculated between the two bound vortex points since the distance is usually a fixed value, while δ will be unity when the distance equation is used for calculating the free vortex induced velocity. This term is designed to prevent the effect of the free vortex being too close to any bound vortex or any other free vortex. Based on the work of Ref. [28], the vortex core distance v_{core} is defined as follows:

$$v_{core} = 1.3c\Delta t^*, \tag{6}$$

where Δt^* is the non-dimensional time step. The self induced velocity term on the left hand side of Equation (2) can be expressed at the control point of each panel. The induced velocity on control point i due to the bound vortex on panel j is represented as an influence coefficient:

$$a_{ij} = \left(\frac{1}{2\pi r_{ij}^2}(z_i - z_j), -\frac{1}{2\pi r_{ij}^2}(x_i - x_J)\right) \cdot \vec{n}_i \tag{7}$$

For panel i, the induced velocity from all the panels with total N bound vortex elements, along with the latest wake vortex (trailing edge vortex) with Γ_w can be written as follows:

$$q_i = a_{i1}\Gamma_1 + a_{i2}\Gamma_2 + \cdots + a_{iN}\Gamma_N + a_{itev}\Gamma_{tev} \tag{8}$$

This self-induced velocity normal to the panel from bound vortices and the latest TEV need to be balanced by the total effect of downwash normal to the panel. As a result, at every time step, we can form a matrix equation with $N+1$ unknowns: $\Gamma_1, \Gamma_2, \ldots \Gamma_N, \Gamma_{TEV}$. The above equation with N panels only provides N equations, so one additional equation to form the final matrix equation will be needed. In this case, the final equation is the Kelvin condition, which implies that the bound circulation strength at the current time step with the newly shed TEV strength should be the same as the sum of the bound circulation strength at the last time step. This fulfills the original statement that the circulation remains constant within a closed contour. The Kelvin condition thus can be written mathematically as:

$$\sum \Gamma_b(t - \Delta t) = \sum \Gamma_b(t) + \Gamma_{TEV} \tag{9}$$

The entire matrix equation thus becomes

$$\begin{bmatrix} a_{11} & a_{12} & \cdots & a_{1N} & a_{1tev} \\ a_{21} & a_{22} & \cdots & a_{2N} & a_{2tev} \\ \cdots & \cdots & \cdots & \cdots & \cdots \\ a_{N1} & a_{N2} & \cdots & a_{NN} & a_{Ntev} \\ 1 & 1 & \cdots & 1 & 1 \end{bmatrix} \begin{bmatrix} \Gamma_1 \\ \Gamma_2 \\ \cdots \\ \Gamma_N \\ \Gamma_{TEV} \end{bmatrix} = \begin{bmatrix} -Wn_1 \\ -Wn_2 \\ \cdots \\ -Wn_N \\ \sum \Gamma_b(t - \Delta t) \end{bmatrix} \tag{10}$$

The matrix of the a_{ij} term is commonly referred to as the influence matrix, similar to the influence matrix used in other panel methods or the Vortex Lattice Method. The downwash normal to the panel, Wn_i, on the right-hand side can be attributed to the effect of freestream velocity, translational motion of airfoil, pitching motion of airfoil, and the total induced velocity from the free vortices except for the latest shedding TEV, the strength of which, has not yet been calculated. The downwash, Wn_i, on the ith panel can be expressed as:

$$Wn_i = W_i \cdot \vec{n}_i = (W_i^{U_0} + W_i^{U_{rel}} + W_i^{\dot{\alpha}} + W_i^{FV}) \cdot \vec{n}_i \tag{11}$$

Here, the four W terms represent the cntributions from the free stream, the airfoil translational motion, the airfoil pitching motion and the free vortices in the flowfield excluding the latest TEV. These terms can be expressed as follows:

$$W_i^{U_0} = U_0\vec{i} + W_0\vec{k} \tag{12}$$

$$W_i^{U_{rel}} = -\dot{X}_0\vec{i} - \dot{Z}_0\vec{k} \tag{13}$$

$$W_i^{\dot{\alpha}} = -(z_{i,bfr} - z_{p,bfr})\dot{\alpha}\vec{i}_{bfr} + (x_{i,bfr} - x_{p,bfr})\dot{\alpha}\vec{k}_{bfr} \tag{14}$$

$$W_i^{FV} = u_w\vec{i} + w_w\vec{k} \tag{15}$$

In this expression, U_0 and W_0 are the freestream velocity components in the X and Z directions in the inertial frame, and $\dot{X}_0$ and $\dot{W}_0$ are the linear velocity components of the airfoil pivot point in the X and Z directions in the inertial frame. The rotational effect is easier to be expressed using the body-fixed frame. For this purpose, we define $x_{i,bfr}$ and $z_{i,bfr}$ as the control-point coordinates of panel i and $x_{p,bfr}$ and $z_{p,bfr}$ as the pivot-point coordinates, expressed in the body-fixed frame. The total induced velocity from the free vortices except for the latest TEV is expressed using u_w and w_w, which is obtained using Biot-Savart law. It is to be noted that for the situations involving unsteady airfoil kinematics, the reference frames, namely the Inertial frame (IFR) and the Body-fixed frame (BFR) will be used wherever appropriate.

The core of the unsteady lumped vortex element (LVE) method is to solve the influence matrix Equation (10) at every time step to get the bound vortex strength distribution and determine the newly shed TEV strength. In the work of Narsipur [1], the newly shed TEV position is predetermined using the velocity of the airfoil trailing edge and that of the previously shed TEV. At every time step, the latest TEV strength and the bound vortex strength is calculated using the influence matrix equation obtained using this position. Once released, the strengths of the free vortices remain unchanged while their positions are updated using the induced velocity and free stream velocity.

B. State Variable form of LVE

A typical state variable form equation can be expressed as follows :

$$\frac{du}{dt} = f(u, p, t) \tag{16}$$

The u is the state vector, which contains all the terms of our interest in a problem. In the current method, the variables we are interested in every time step include the positions of all the free vortices, their strengths, the positions of bound vortices, their strengths and the airfoil position. Thus, we can classify the state variables into three groups: airfoil, free vortices, and bound vortices. For the airfoil group, the state variables we are interested in are its position components, velocities, pitch angle, and angular velocity. This results in our airfoil state being expressed as follows:

$$\vec{U}_{AF} = [X_0 \ Z_0 \ \dot{X}_0 \ \dot{Z}_0 \ \alpha \ \dot{\alpha}]^T \tag{17}$$

For each free vortex, the state will be:

$$\vec{U}_{fv} = [x_{fv} \ z_{fv} \ \Gamma_{fv}]^T \tag{18}$$

And for each bound vortex, the state will be:

$$\vec{U}_{bv} = [x_{bv} \ z_{bv} \ \Gamma_{bv}]^T \tag{19}$$

With the state variables identified, the corresponding functions to express the time derivative of all the state variables are needed in order to obtain the state variable equation. For the state variables of the airfoil, the time derivative terms will be:

$$\frac{d\vec{U}_{AF}}{dt} = [\dot{X}_0 \ \dot{Z}_0 \ \ddot{X}_0 \ \ddot{Z}_0 \ \dot{\alpha} \ \ddot{\alpha}]^T \tag{20}$$

These terms represent linear velocity and acceleration and angular velocity and acceleration. In situations where the airfoil is undergoing a prescribed motion, these terms can be determined by using the known motion function. For a more general case, such as that of the aeroelastic oscillation of an airfoil, these terms can be determined using the aerodynamic loads.

For the free vortex state variables, the time derivative terms will be :

$$\frac{d\vec{U}_{fv}}{dt} = \begin{bmatrix} \dot{x}_{fv} \\ \dot{z}_{fv} \\ \dot{\Gamma}_{fv} \end{bmatrix} = \begin{bmatrix} u_{bv} + u_{fv} + U_0 \\ w_{bv} + w_{wv} + W_0 \\ 0 \end{bmatrix} \tag{21}$$

The first two terms on the right-hand side of the first two equations represent the velocity of the free vortices. These terms are determined using the induced velocity from all the bound vortices (u_{bv}, w_{bv}) and from all the free vortices (u_{fv}, w_{fv}) via Biot-Savart law, and also using the free stream velocity effect (U_0, W_0). The rate of change of strength will be zero for the free vortices. The latest vortex that is about to leave the airfoil surface will require some special treatment to determine its strength and will be discussed later.

For the bound vortex state variables, the time derivative terms become:

$$\frac{d\vec{U}_{bv}}{dt} = \begin{bmatrix} \dot{x}_{bv} \\ \dot{z}_{bv} \\ \dot{\Gamma}_{bv} \end{bmatrix} \tag{22}$$

Since the positions of bound vortices and the control points are directly linked to the airfoil state variables, their velocities can be determined by the same information as for the airfoil state variables. For deforming airfoils, the rate of deformation will also need to be considered to express the velocity of the bound vortices. To calculate the rate change of the bound vortex strength, we will need to refer back to Equation (10) and derive the time derivative version of it. The time derivative version of the influence matrix equation will be:

$$\frac{d}{dt}\left(\begin{bmatrix} a_{11} & a_{12} & \cdots & a_{1N} & a_{1tev} \\ a_{21} & a_{22} & \cdots & a_{2N} & a_{2tev} \\ \cdots & \cdots & \cdots & \cdots & \cdots \\ a_{N1} & a_{N2} & \cdots & a_{NN} & a_{Ntev} \\ 1 & 1 & \cdots & 1 & 1 \end{bmatrix}\right)\begin{bmatrix} \Gamma_1 \\ \Gamma_2 \\ \cdots \\ \Gamma_N \\ \Gamma_{TEV} \end{bmatrix} + \begin{bmatrix} a_{11} & a_{12} & \cdots & a_{1N} & a_{1tev} \\ a_{21} & a_{22} & \cdots & a_{2N} & a_{2tev} \\ \cdots & \cdots & \cdots & \cdots & \cdots \\ a_{N1} & a_{N2} & \cdots & a_{NN} & a_{Ntev} \\ 1 & 1 & \cdots & 1 & 1 \end{bmatrix}\begin{bmatrix} \dot{\Gamma}_1 \\ \dot{\Gamma}_2 \\ \cdots \\ \dot{\Gamma}_N \\ \dot{\Gamma}_{TEV} \end{bmatrix} = \begin{bmatrix} -\dot{W}n_1 \\ -\dot{W}n_2 \\ \cdots \\ -\dot{W}n_N \\ 0 \end{bmatrix} \tag{23}$$

It should be noted that this equation governs the rate change of the bound vortex strength and also that of the TEV that is about to be shed. Although this equation seems to require a time derivative version of the influence matrix, in this equation, the latest TEV will initially have zero strength, and the term $\dot{a}_{ij}$ will be zero given that the airfoil does not deform. This significantly simplifies the time derivative influence matrix equation as:

$$\begin{bmatrix} a_{11} & a_{12} & \cdots & a_{1N} & a_{1tev} \\ a_{21} & a_{22} & \cdots & a_{2N} & a_{2tev} \\ \cdots & \cdots & \cdots & \cdots & \cdots \\ a_{N1} & a_{N2} & \cdots & a_{NN} & a_{Ntev} \\ 1 & 1 & \cdots & 1 & 1 \end{bmatrix}\begin{bmatrix} \dot{\Gamma}_1 \\ \dot{\Gamma}_2 \\ \cdots \\ \dot{\Gamma}_N \\ \dot{\Gamma}_{TEV} \end{bmatrix} = \begin{bmatrix} -\dot{W}n_1 \\ -\dot{W}n_2 \\ \cdots \\ -\dot{W}n_N \\ 0 \end{bmatrix} \tag{24}$$

By solving this equation, the rate change of bound vortex strength can be obtained. The right-hand side of the equation can be realized as the time derivative term of the downwash normal to the airfoil panel. Based on the previous derivation of the Wn term, we can write it as :

$$Wn_i = f(U_0, W_0, \dot{X}_0, \dot{Z}_0, x_{i,bfr}, z_{i,bfr}, x_{p,bfr}, z_{p,bfr}, \dot{\alpha}, u_w, w_w, \vec{n}_i) \tag{25}$$

The time derivative of this term can further be expressed using the gradient:

$$\dot{W}n_i = \frac{\partial f}{\partial U_0}\dot{U}_0 + \frac{\partial f}{\partial W_0}\dot{W}_0 + \frac{\partial f}{\partial \dot{x}_0}\ddot{X}_0 + \cdots + \frac{\partial f}{\partial u_w}\dot{u}_w + \frac{\partial f}{\partial w_w}\dot{w}_w + \frac{\partial f}{\partial \vec{n}_i}\dot{\vec{n}}_i \tag{26}$$

The gradient terms can be calculated using any automatic differentiation tools in modern computing languages. In this work, the JuliaDiff/ForwardDiff package [29] is used to calculate all the gradient terms, while all the time derivative terms are calculated using the current state variables. Importantly, the time derivative of the normal vector of each panel also needs to be calculated if the inertial frame is used, as the normal vector will change due to airfoil motion. The time derivative of the induced velocity terms due to the free vortex: $(\dot{u}_w, \dot{w}_w)$ come from the time derivative of the induced velocity function, and from Equations (3) and (4):

$$\vec{u}_{ij} = f(x_i, z_i, x_j, x_J, \Gamma_j) \tag{27}$$

The time derivative version of the induced velocity thus becomes:

$$\vec{u}_{ij} = \frac{\partial f}{\partial x_i}\dot{x_i} + \frac{\partial f}{\partial z_i}\dot{z_i} + \frac{\partial f}{\partial x_j}\dot{x_j} + \frac{\partial f}{\partial z_j}\dot{z_j} + \frac{\partial f}{\partial \Gamma_j}\dot{\Gamma}_j \tag{28}$$

All the time derivative terms can be derived from the state variables at the current time steps.

With the expression $\dot{W}_n$ determined, the last thing we need to do is to determine the initial shedding TEV position so that we can calculate the influence matrix. The current mechanism of TEV shedding assumes that at every time step, the newest shedding TEV is released at some distance behind the trailing edge, which is defined by

$$\vec{x}_{newTEV} = \vec{x}_{TE} + \vec{U}_0 \Delta t \tag{29}$$

Here, $\vec{x}_{newTEV}$ is the initial position of the new TEV, $\vec{x}_{TE}$ is the trailing edge position at the current time step, and $\vec{U}_0$ is the free stream velocity vector. This initial TEV position is also used to evaluate the influence matrix, and thus the rate change of the bound vortices and the newest shedding vortex at the current time step. In the TEV shedding mechanism, a new TEV will be shed at every time step at the predetermined initial position given by (29). Its velocity is determined by the induced velocity due to all the bound vortices, other free vortices, and the free stream velocity. It's strength is assumed to be zero initially and the final value at the next time step depends on $\dot{\Gamma}_{TEV}$ from Equation (24). Starting from the next time step, the strength of this TEV will not change anymore, and its velocity will be determined using the same mechanism. Finally, the entire state variable form equations can be expressed by merging all the time derivative expressions of the states of the airfoil, free vortices, and bound vortices.

C. The Unsteady Loads on the Airfoil and LESP

Using the state variable formulation presented above, the bound vortex strength can be solved at every time step. To obtain the unsteady aerodynamic forces and moment, the unsteady Bernoulli equation is used to derive the pressure distribution.

$$\Delta p(x) = \rho \left[\left(U \cos\theta + \dot{h} \sin\theta + u_{ind}(x) \right) \gamma(x) + \frac{\partial}{\partial t} \int_{x'=0}^{x} \gamma(x') dx' + \dot{\Gamma}_{lev} \right] \tag{30}$$

In the current LVE model, the pressure difference at panel i can be rewritten as :

$$\Delta p_i = \rho \left(\vec{U}_0 - \vec{U}_{rel} - \dot{\alpha} \times \vec{r} + \vec{u_w} \right) \cdot \vec{\tau}_i \frac{\Gamma_i}{l_i} + \frac{\partial}{\partial t} \sum_{k=1}^{k=i} \Gamma_k + \dot{\Gamma}_{lev} \tag{31}$$

Here, Γ_i refers to the bound vortex strength of the ith panel, l_i refers to the length of the ith panel, and $\vec{u}_w$ refers to the induced velocity vector due to all the free vortices. In (30) and (31), the third term explicitly takes into account the effect of circulation production due to LEV shedding on the unsteady loads of the airfoil. The first term is the circulatory term and relies on the velocity tangential to the panel and the bound vortex sheet strength while the second term is refereed to as the apparent mass term.

The normal force coefficient can be derived by summing the pressure difference, and is given as:

$$C_n = 2 \frac{\sum_{i=1}^{N} \Delta p_i l_i}{\rho U_\infty^2 c} \tag{32}$$

The LESP can be defined using the following equation [30]:

$$LESP(t) = \frac{1.13 \Gamma_1(t)}{U_\infty(t) c [\cos^{-1}(1 - 2l_1/c) + \sin(\cos^{-1}(1 - 2l_1/c))]} \tag{33}$$

And the corresponding suction force coefficient can be derived from the LESP:

$$C_s = 2\pi LESP^2(t) \tag{34}$$

Using the normal and the suction force coefficients the lift and drag coefficients can be evaluated as:

$$C_L = C_N \cos\alpha + C_S \sin\alpha \tag{35}$$

$$C_D = C_N \sin\alpha - C_S \cos\alpha \tag{36}$$

Moment coefficient can be calculated using the equation,

$$C_m = -2 \frac{\sum_{i=1}^{N} \Delta p_i l_i (x_i - x_{pivot})}{\rho U_\infty^2 c^2} \tag{37}$$

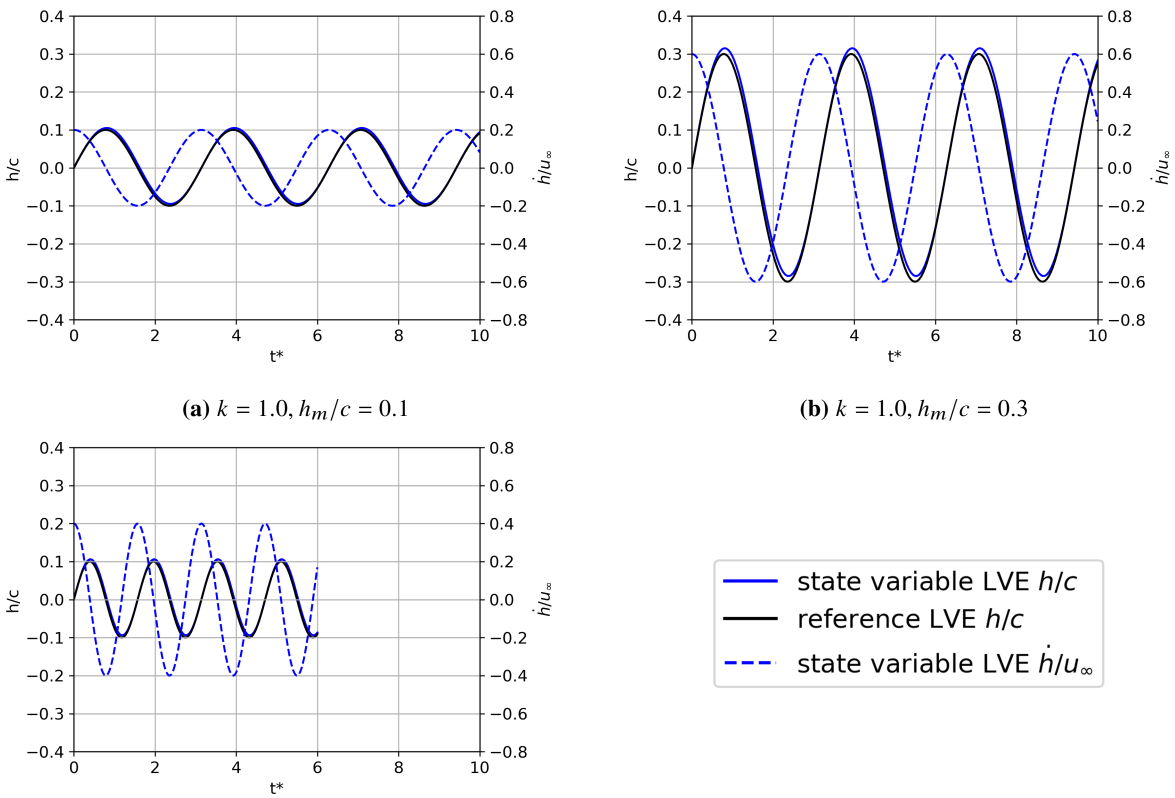

(a) $k = 1.0, h_m/c = 0.1$ **(b)** $k = 1.0, h_m/c = 0.3$

(c) $k = 2.0, h_m/c = 0.1$ **(d) legend of the motion**

Fig. 2 Motion histories for the state-variable form LVE and the reference LVE method.

III. Results

In this section, we compare the results from the current state-variable form LVE to the LVE method originated from the work of Narsipur [1] (referred to as the reference LVE method henceforth). We consider three harmonic plunge motions, with $k = 1.0$, $h_m/c = 0.1$, $k = 1.0$, $h_m/c = 0.3$, and $k = 2.0$, $h_m/c = 0.1$, where k is the reduced frequency and h_m/c is the non-dimensional plunge amplitude. The plunge displacement and velocity are presented in figure 2, with two displacement history curves, one from the current state variable form and the other from the exact input for the reference LVE method. For each motion, we compare the aerodynamics loads including C_l, C_d, C_m, and $LESP$ history and also the vortex distribution to compare the difference between the two solvers. The state-variable form LVE method is implemented in the programming language Julia 1.6.1 and the differential equation solver package from Ref. [31] is used to solve the state variable equation. The legend used in this section are shared among the three motions and is shown in Fig. 3.

Fig. 3 Legends used in this section for load histories (top row) and vortex-distribution plots (bottom row).

A. $k = 1.0, h_m/c = 0.1$ Plunge Motion

The load and LESP history for this motion is presented in Fig. 4 and the snapshots of vortex distribution are shown in Fig. 5. From these figures, we can see that there is no LEV shedding and thus all the aerodynamic load histories become harmonic distributions just like the motion history. The lift coefficient oscillates between a positive maximum and a negative minimum. Meanwhile, the drag is always negative, indicating that this motion actually results in a thrust force on the airfoil. From Fig. 4, we can notice that the frequency of the lift, moment, and LESP are the same, but the frequency of the drag is twice this value. This suggests that the drag force experienced by the airfoil for a positive heave displacement is similar to a corresponding negative displacement, while the lift force has a different direction.

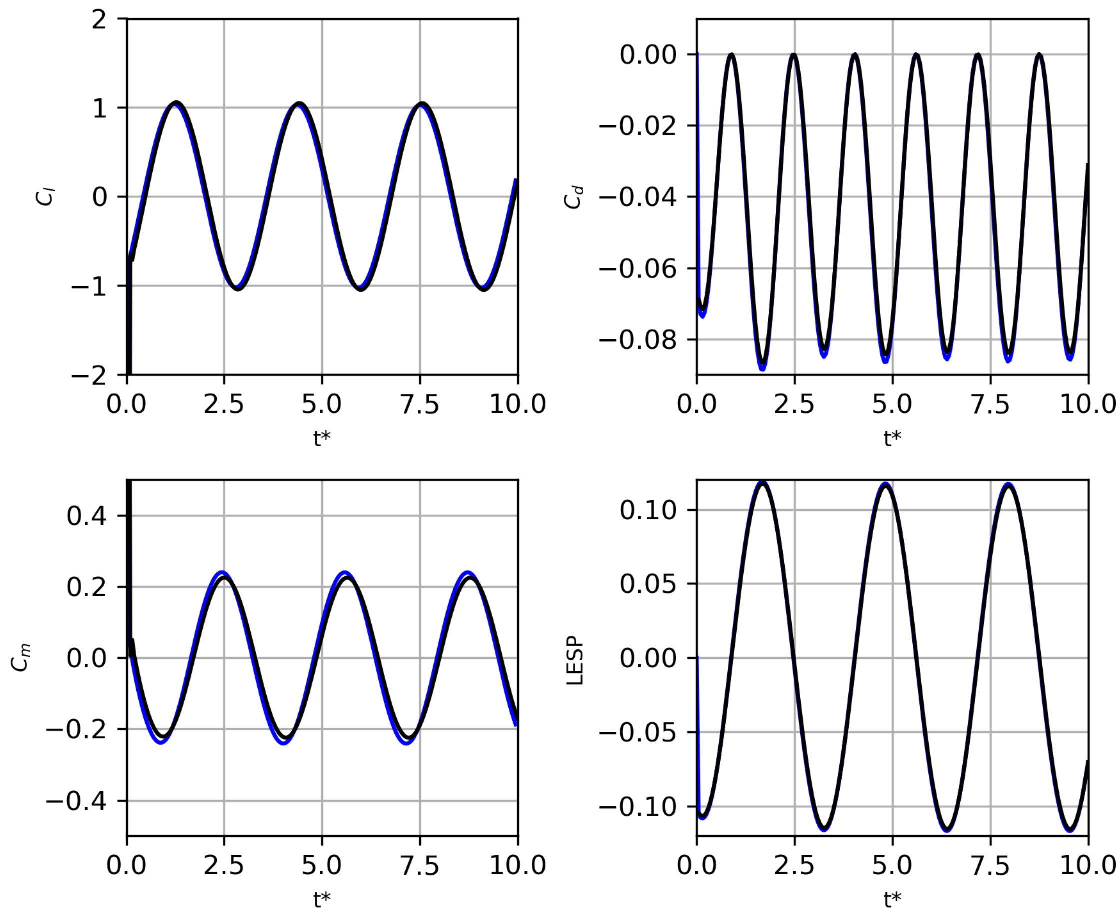

Fig. 4 Comparison of load histories from the state-variable LVE model and the reference LVE method for harmonic plunge motion with $k = 1.0, h_m/c = 0.1$

When comparing the results between the state variable form LVE and the reference LVE method, it is evident that the lift, drag, and moment coefficient histories match well with the results from the reference LVE method. When the airfoil is at the maximum heave displacement, the state variable form method shows slightly higher peak values for the drag and moment coefficients compared to the reference LVE method. From the vortex plots, it can be observed that the state variable LVE has a very similar result to that of the reference LVE method, except for some minor differences in the vortex positions at various time instants. This reveals that the strengths of the TEVs and the overall bound vortex strength distribution at each time step should be similar, thus resulting in a very similar wake roll-up pattern.

B. $k = 1.0, h_m/c = 0.3$ Plunge Motion

The load and LESP history for this higher amplitude motion are presented in Fig. 6 and the snapshots of vortex distribution are shown in Fig. 7. From these figures, we can see that there is no LEV shedding and thus all the aerodynamic load history becomes a harmonic distribution just like the motion. In the real scenario, this motion actually might have LEV shedding. LEV shedding has not been modeled in the current simulations and will be considered in future work.

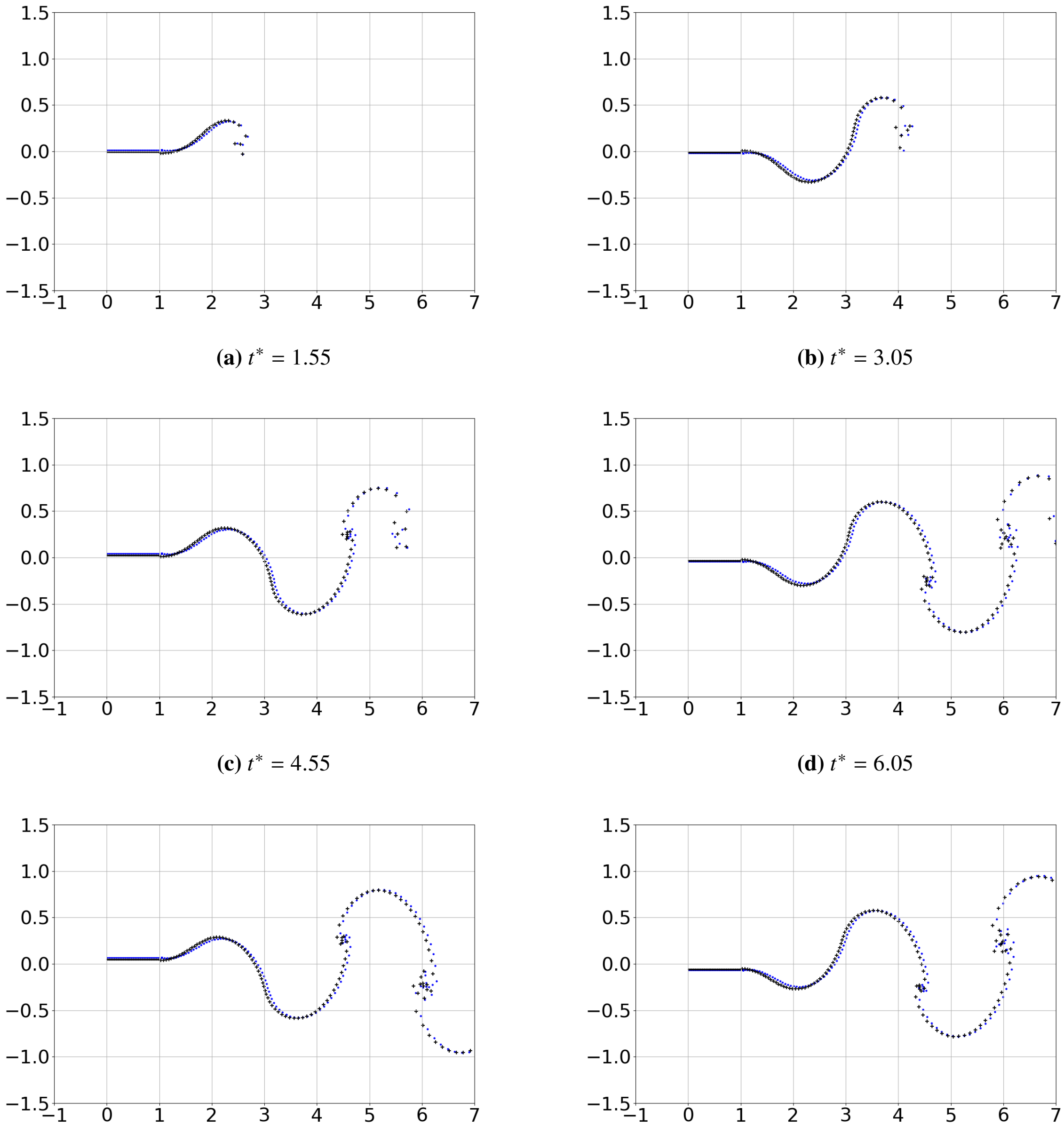

(a) $t^* = 1.55$ **(b)** $t^* = 3.05$

(c) $t^* = 4.55$ **(d)** $t^* = 6.05$

(e) $t^* = 7.55$ **(f)** $t^* = 9.05$

Fig. 5 Co-plot of vorticity distributions from the state-variable LVE model and the reference LVE method for harmonic plunge motion with $k = 1.0, h_m/c = 0.1$

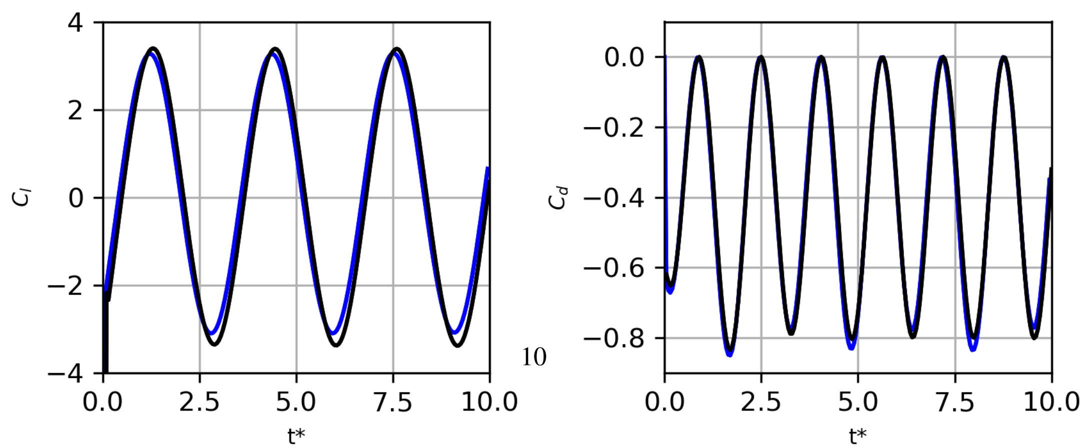

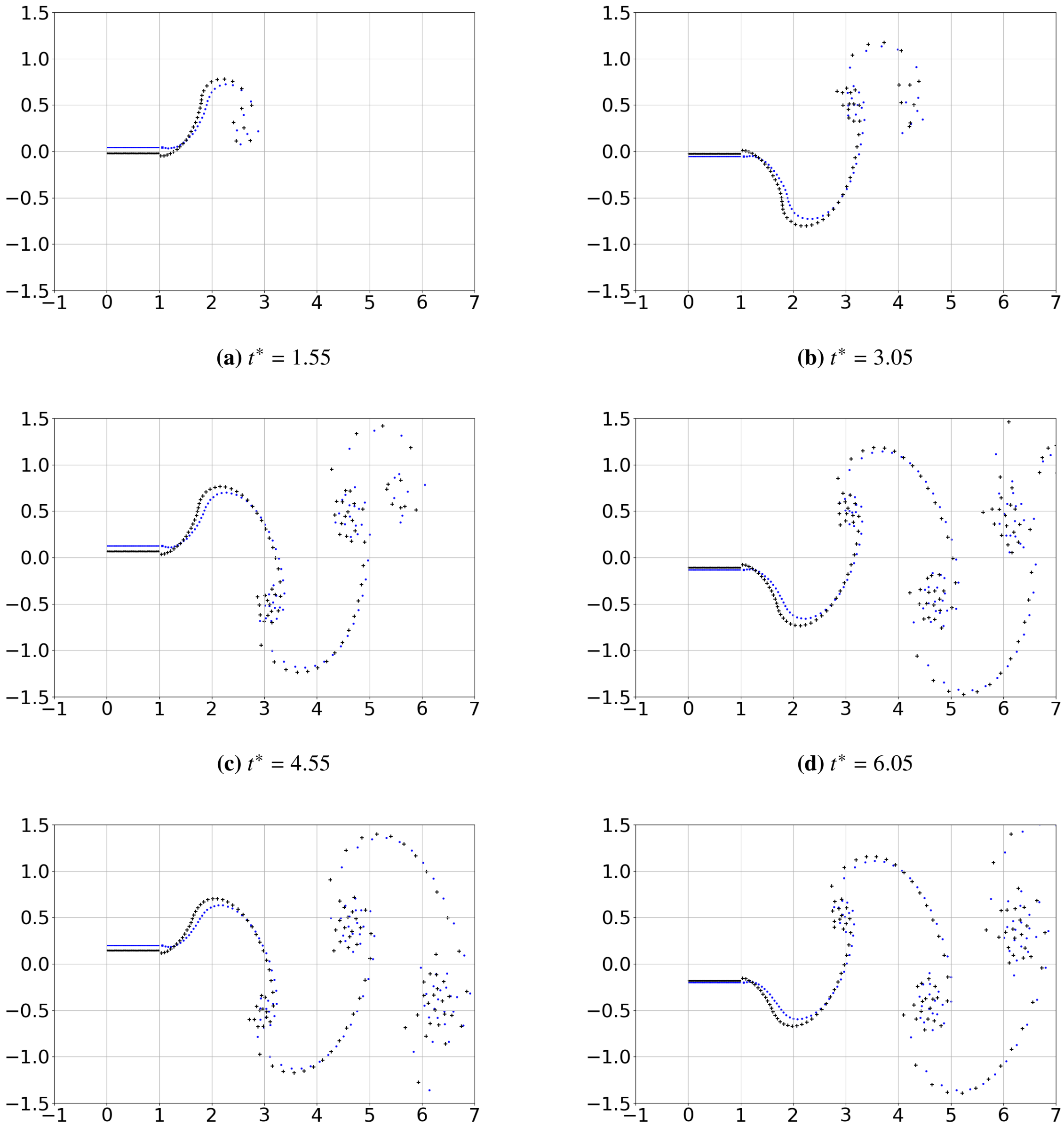

(a) $t^* = 1.55$ **(b)** $t^* = 3.05$ **(c)** $t^* = 4.55$ **(d)** $t^* = 6.05$ **(e)** $t^* = 7.55$ **(f)** $t^* = 9.05$

Fig. 7 Co-plot of vorticity distributions from the state-variable LVE model and the reference LVE method for harmonic plunge motion with $k = 1.0$, $h_m/c = 0.3$

The lift, drag, and moment coefficient history from the current model matches well with the results from the reference LVE method, with the peak value difference being slightly larger than the previous case. From the vortex plots, we can observe that the bound vortex positions from the two methods are slightly different from each other. This mismatch can also be observed from the motion history plot in fig. 2. This problem arises from the fact that the reference LVE method takes the exact position input, while in the state variable form method, the position is calculated via the provided motion velocity. However, even with this difference, the wake structures are still in good agreement with each other. Moreover, all the aerodynamic load and LESP histories are captured by the state variable form solver in good agreement with the reference results.

C. $k = 2.0, h_m/c = 0.1$ Plunge Motion

The load and LESP history for this higher frequency motion is presented in Fig. 8 and the snapshots of vortex distribution are shown in Fig. 9. From these figures, it can be seen that there is no LEV shedding and that all the aerodynamic load histories are harmonic distributions just like the motion. Similar to the previous case, the frequency of the lift, moment, and LESP is half of the drag coefficient, and the plunge motion also generates thrust on the airfoil rather than the drag.

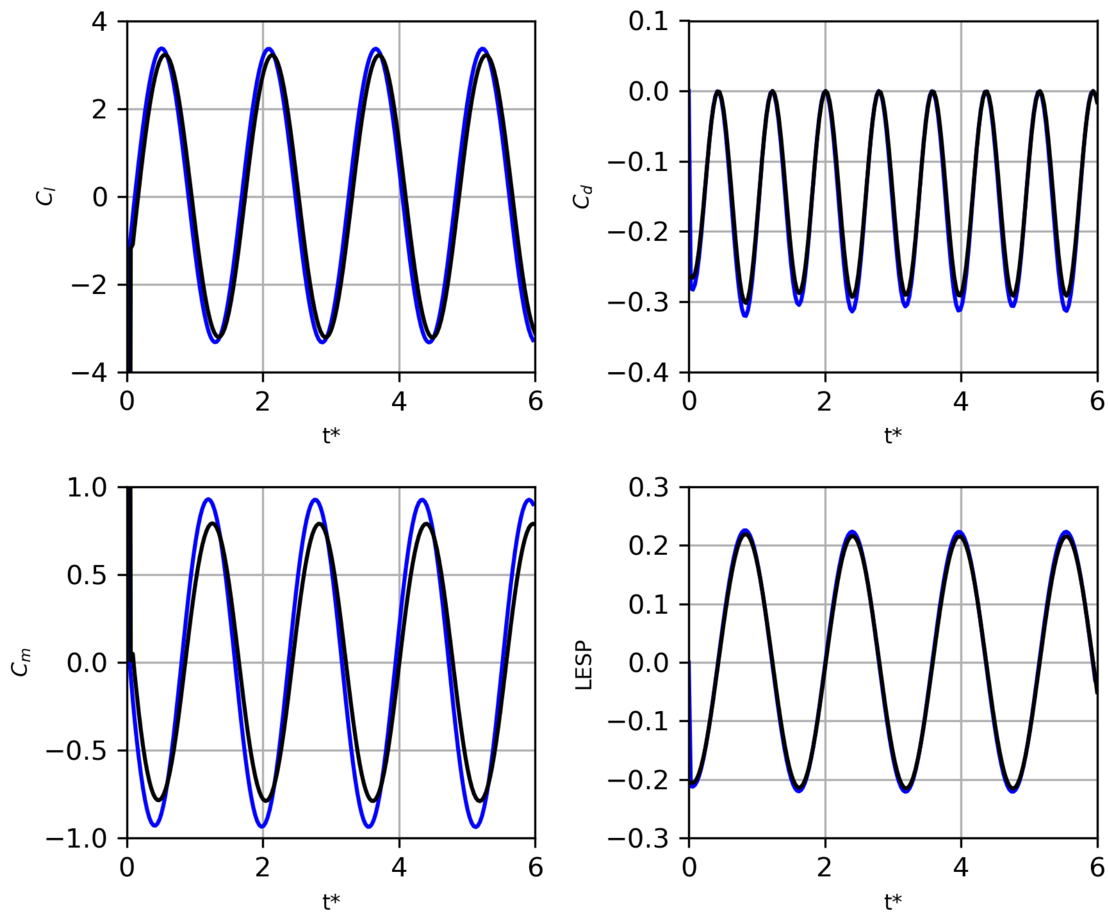

Fig. 8 Comparison of load histories from the state-variable LVE model and the reference LVE method for harmonic plunge motion with $k = 2.0, h_m/c = 0.1$

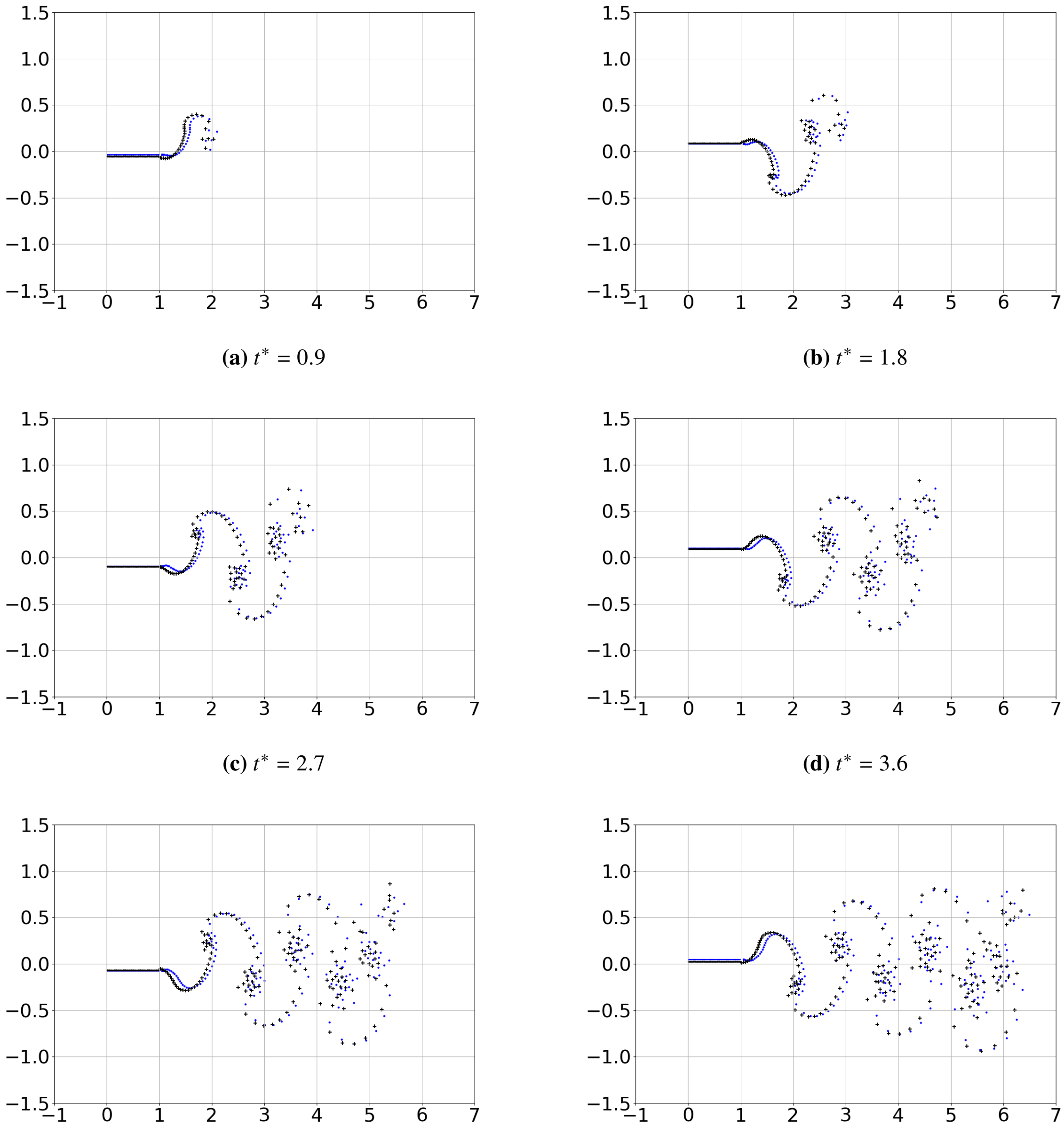

(a) $t^* = 0.9$

(b) $t^* = 1.8$

(c) $t^* = 2.7$

(d) $t^* = 3.6$

(e) $t^* = 4.5$

(f) $t^* = 5.4$

Fig. 9 Co-plot of vorticity distributions from the state-variable LVE model and the reference LVE method for harmonic plunge motion with $k = 1.0, h_m/c = 0.1$

The lift, drag and moment coefficient history along with LESP from the state-variable form method match well with the reference results. The difference between the two methods in terms of the peak values of the quantities seems to be larger than the previous two cases. From the vortex plots, we can see that wake roll-up patterns are very similar between the two methods. The small differences in TEV positions, along with the differences in the bound vortex positions due to integration errors may be the reason for the difference in aerodynamic load peak value. The three case studies indicate that the state-variable form LVE shows some promise in accurately capturing the unsteady aerodynamic characteristics and wake patterns of an unsteady airfoil.

IV. Conclusion

In this research, we present the idea of using the lumped-vortex element (LVE) model with trailing edge vortex shedding to simulate the flow field around an airfoil undergoing an unsteady motion. Based on the earlier work of the reference LVE method from Narsipur et al. [26] we propose that a state variable form using the conventional LVE model can be derived and that all the time derivatives of the variables of interest can be expressed using other state variables. The state variable form model has the potential to be easily integrated with other structural models to simulate aeroelasticity problems. Moreover, it can be easily tailored to use higher-order integration methods for time stepping. In this work, we identified the state variables of interest for the flow field, and derived the expressions for all the time derivative terms as functions of the state variables. The time derivative version of the influence matrix equation from the reference LVE has been shown to be the critical part of the current model and governs the rates of changes of the airfoil bound circulation and the nascent TEV strengths. In order to solve this equation, a TEV shedding mechanism based on a time derivative version of the Kelvin condition is also proposed in this work.

The initial testing of the current model using three different harmonic plunge motions show promising results when compared to the results of the reference LVE model. The aerodynamic load history and LESP history are similar between the two methods for all the cases, indicating that the state variable form model can precisely capture the vortex-dominated flow field behind an unsteady airfoil. The Vortex distribution plots from the two models show identical wake roll-up patterns. The minor differences between the results from the two models may be attributed to the errors caused by the numerical integration schemes. The future workon this research will include improving the TEV shedding mechanism and introducing a model for LEV shedding from the airfoil. It is also proposed to investigate the possibility of improving the efficiency of the computer implementation of the method in order to reduce the computational cost.

V. Acknowledgment

The authors gratefully acknowledge funding support for this research from the National Science Foundation under Award No. CMMI-2015983 and program officer Dr. Robert Landers.

References

[1] Narsipur, S., "Low-Order Modeling of Dynamic Stall on Airfoils in Incompressible Flow," Ph.D. thesis, North Carolina State University, 2017.

[2] Tietjens, O. K. G., and Prandtl, L., *Applied Hydro- and Aeromechanics: Based on Lectures of L. Prandtl.*, Courier Corporation., 1934.

[3] Ellington, C. P., van den Berg, C., Willmott, A. P., and Thomas, A. L. R., "Leading-edge vortices in insect flight." *Nature*, Vol. 384, 1996, pp. 626–630. https://doi.org/10.1038/384626a0.

[4] Willmott, A. P., and Ellington, C. P., "The mechanics of flight in the hawkmoth Manduca sexta. I. Kinematics of hovering and forward flight." *Journal of Experimental Biology*, Vol. 200, No. 21, 1997, pp. 2705–2722. https://doi.org/10.1242/jeb.200.21.2705.

[5] Dickinson, M. H., Lehmann, F.-O., and Sane, S. P., "Wing Rotation and the Aerodynamic Basis of Insect Flight," *Science*, Vol. 284, No. 5422, 1999, pp. 1954–1960. https://doi.org/10.1126/science.284.5422.1954.

[6] Usherwood, J. R., and Ellington, C. P., "The aerodynamics of revolving wings I. Model hawkmoth wings," *Journal of Experimental Biology*, Vol. 205, No. 11, 2002, pp. 1547–1564. https://doi.org/10.1242/jeb.205.11.1547.

[7] McCroskey, W., *The Phenomenon of Dynamic Stall.*, 1981.

[8] Ekaterinaris, J. A., and Platzer, M. F., "Computational prediction of airfoil dynamic stall," *Progress in Aerospace Sciences*, Vol. 33, No. 11, 1998, pp. 759–846. https://doi.org/10.1016/S0376-0421(97)00012-2.

[9] Jones, K. D., and Platzer, M. F., "On the Prediction of Dynamic Stall Onset on Airfoils in Low Speed Flow," *Unsteady Aerodynamics and Aeroelasticity of Turbomachines*, edited by T. H. Fransson, Springer, Dordrecht, 1998, pp. 797–812.

[10] Geissler, W., and Haselmeyer, H., "Investigation of dynamic stall onset," *Aerospace Science and Technology*, Vol. 10, No. 7, 2006, pp. 590–600. https://doi.org/10.1016/j.ast.2006.05.001.

[11] McCroskey, W., Carr, L., and McAlister, K., "Dynamic Stall Experiments on Oscillating Airfoils," *AIAA Journal*, Vol. 14, No. 1, 1976, pp. 57–63. https://doi.org/10.2514/3.61332.

[12] McCroskey, W. J., "Unsteady Airfoils," *Annual Review of Fluid Mechanics*, Vol. 14, No. 1, 1982, pp. 285–311. https://doi.org/10.1146/annurev.fl.14.010182.001441.

[13] Acharya, M., and Metwally, M. H., "Unsteady pressure field and vorticity production over a pitching airfoil," *AIAA Journal*, Vol. 30, No. 2, 1992, pp. 403–411. https://doi.org/10.2514/3.10931.

[14] Lee, T., and Gerontakos, P., "Investigation of flow over an oscillating airfoil," *Journal of Fluid Mechanics*, Vol. 512, 2004, p. 313–341. https://doi.org/10.1017/S0022112004009851.

[15] Gupta, R., and Ansell, P. J., "Unsteady Flow Physics of Airfoil Dynamic Stall," *AIAA Journal*, Vol. 57, No. 1, 2019, pp. 165–175. https://doi.org/10.2514/1.J057257.

[16] Spentzos, A., Barakos, G., Badcock, K., Richards, B., Wernert, P., Schreck, S., and Raffel, M., "Investigation of Three-Dimensional Dynamic Stall Using Computational Fluid Dynamics," *AIAA Journal*, Vol. 43, No. 5, 2005, pp. 1023–1033. https://doi.org/10.2514/1.8830.

[17] Morris, W. J., and Rusak, Z., "Stall onset on aerofoils at low to moderately high Reynolds number flows," *Journal of Fluid Mechanics*, Vol. 733, 2013, p. 439–472. https://doi.org/10.1017/jfm.2013.440.

[18] Ramesh, K., Gopalarathnam, A., Granlund, K., Ol, M., and Edwards, J., "Discrete-vortex method with novel shedding criterion for unsteady airfoil flows with intermittent leading-edge vortex shedding," *Journal of Fluid Mechanics*, Vol. 751, 2014, pp. 500–538. https://doi.org/10.1017/jfm.2014.297.

[19] Narsipur, S., Hosangadi, P., Gopalarathnam, A., and Edwards, J. R., "Variation of leading-edge suction during stall for unsteady aerofoil motions," *Journal of Fluid Mechanics*, Vol. 900, 2020. https://doi.org/10.1017/jfm.2020.467.

[20] SureshBabu, A., Ramesh, K., and Gopalarathnam, A., "Model Reduction in Discrete-Vortex Methods for Unsteady Airfoil Flows," *AIAA Journal*, Vol. 57, No. 4, 2019, pp. 1409–1422. https://doi.org/10.2514/1.J057458.

[21] Medina, A., SureshBabu, A., Rockwood, M. P., Gopalarathnam, A., and Anwar, A., "Theoretical and Experimental Study of Wake Encounters on Unsteady Airfoils," AIAA Paper 2019-0898, January 2019.

[22] SureshBabu, A., Medina, A., Rockwood, M., Bryant, M., and Gopalarathnam, A., "Theoretical and experimental investigation of an unsteady airfoil in the presence of external flow disturbances," *Journal of Fluid Mechanics*, Vol. 921, 2021, p. A21. https://doi.org/10.1017/jfm.2021.484.

[23] Mistele, A., SureshBabu, A., and Gopalarathnam, A., "Inviscid Model for Unsteady Multi-Airfoil Configurations with Leading-Edge Vortex Shedding," AIAA Paper 2021-1824, January 2021. https://doi.org/10.2514/6.2021-1824.

[24] Faure, T., Dumas, L., and Montagnier, O., "Numerical study of two-airfoil arrangements by a discrete vortex method," *Theoretical and Computational Fluid Dynamics*, Vol. 34, 2020, pp. 79–103. https://doi.org/10.1007/s00162-019-00511-0.

[25] SureshBabu, A., and Gopalarathnam, A., "Low-order modeling of dynamic stall in vertical-axis wind turbines," AIAA Paper 2019-3585, June 2019. https://doi.org/10.2514/6.2019-3585.

[26] Narsipur, S., Gopalarathnam, A., and Edwards, J. R., "Low-Order Model for Prediction of Trailing-Edge Separation in Unsteady Flow," *AIAA Journal*, Vol. 57, No. 1, 2019, pp. 191–207. https://doi.org/10.2514/1.J057132.

[27] Ramesh, K., Murua, J., and Gopalarathnam, A., "Limit-cycle oscillations in unsteady flows dominated by intermittent leading-edge vortex shedding," *Journal of Fluids and Structures*, Vol. 55, 2015, pp. 84–105. https://doi.org/https://doi.org/10.1016/j.jfluidstructs.2015.02.005, URL https://www.sciencedirect.com/science/article/pii/S0889974615000468.

[28] "Vortex methods for flow simulation," *Journal of Computational Physics*, Vol. 37, No. 3, 1980, pp. 289–335. https://doi.org/https://doi.org/10.1016/0021-9991(80)90040-6.

[29] Revels, J., Lubin, M., and Papamarkou, T., "Forward-Mode Automatic Differentiation in Julia," *arXiv:1607.07892 [cs.MS]*, 2016. URL https://arxiv.org/abs/1607.07892.

[30] Aggarwal, S., "An inviscid numerical method for unsteady flows over airfoils and wings to predict the onset of leading edge vortex formation," , 2017.

[31] Rackauckas, C., and Nie, Q., "Differentialequations.jl–a performant and feature-rich ecosystem for solving differential equations in julia," *Journal of Open Research Software*, Vol. 5, No. 1, 2017.